# Simulation of K-type and H-type Transition Using the Nonlinear One-Way Navier-Stokes Approach

Michael K. Sleeman[1], Matthew T. Lakebrink[2], and Tim Colonius[1]

[1] Department of Mechanical and Civil Engineering, California Institute of Technology, Pasadena, USA
msleeman@caltech.edu
[2] Boeing Research & Technology, Hazelwood, MO, USA

**Abstract.** In principle, transition to turbulence can be studied using direct numerical simulation (DNS) and large eddy simulation (LES), but these approaches are limited by their large computational cost. The Nonlinear One-Way Navier-Stokes (NOWNS) equations have recently been developed and applied to study the early stages of boundary layer transition, and it was demonstrated that they can accurately replicate DNS results with similar accuracy to the nonlinear parabolized stability equations (NPSE) [15]. While having greater computational cost than NPSE, NOWNS is a more robust, convergent parabolization of the governing equations and succeeds for stronger nonlinearity where NPSE fails. In this work, we use NOWNS to reproduce (to the extent possible) the H- and K-type transition scenarios simulated using DNS by Sayadi et al. [14].

**Keywords:** Simulation, boundary layers, laminar-turbulent transition

## 1 Methodology

The OWNS procedure was first developed as a method for constructing well-posed one-way approximations of linear hyperbolic systems with slowly-varying coefficients in the direction of integration [16], allowing the equations to be solved as a spatial-initial-value problem, leading to a reduced computational cost. The framework has also been applied to the Navier-Stokes equations, linearized about a slowly-varying baseflow, to perform linear stability analysis of jets and boundary layer flows [16, 17, 8, 7, 9, 11]. More recently, the OWNS procedure has been extended to support nonlinear effects [15]. We briefly summarize the NOWNS methodology, and refer to Sleeman et al. (2025) for the details [15].

### 1.1 Linear OWNS

We take the compressible Navier-Stokes equations, with constant fluid properties (since we are considering only low-speed flows), as our governing equations. We aim to study disturbances to a time-invariant equilibrium solution (e.g., the Blasius

solution), $\bar{\boldsymbol{q}}$. We linearize about $\bar{\boldsymbol{q}}$ and then consider disturbances that are periodic in time with frequency $\omega$ and in the spanwise direction with wave number $\beta$, such that

$$\boldsymbol{q}'(x,y,z,t) = \sum_{m=-M}^{M} \sum_{n=-N}^{N} \hat{\boldsymbol{q}}_{mn} e^{i(n\beta z - m\omega t)}. \tag{1}$$

We assume infinitesimal disturbance amplitudes in the linear case so that each frequency-wavenumber pair $(m\omega, n\beta)$ can be handled separately. Further, we discretize in the wall-normal direction using 4th-order central finite differences which we represent using $D \approx \partial/\partial y$.

Following discretization, we transform to characteristic variables, $\boldsymbol{\phi}$, and obtain the ordinary differential equation (ODE) $\partial_x \boldsymbol{\phi}_\pm = M\hat{\boldsymbol{\phi}}_\pm + \hat{\boldsymbol{g}}$, where $\hat{\boldsymbol{g}}$ is an arbitrary forcing function. The OWNS projection (OWNS-P) approach allows for the construction of a projection operator, $P$, based on the eigensystem of $M$, which retains the downstream-going modes, yielding the downstream-going solution $\hat{\boldsymbol{\phi}}' = P\hat{\boldsymbol{\phi}}$. We use $P$, along with linearity, to obtain an equation that supports only downstream-going modes $\partial_x \hat{\boldsymbol{\phi}}'_\pm = P[M\hat{\boldsymbol{\phi}}'_\pm + \hat{\boldsymbol{g}}]$. In practice, it is not feasible to apply the exact projection operator, so we instead apply it approximately using a recursive filtering approach [16, 17].

### 1.2 Nonlinear OWNS

To obtain the NOWNS equations, we consider a system of linear OWNS equations, for frequency and wavenumber pairs $(m\omega, n\beta)$, coupled together through the nonlinear term. We treat the nonlinear term as a forcing function, $\hat{\boldsymbol{g}}_{mn}(\boldsymbol{\phi}'_\pm)$, to obtain

$$\frac{\partial \hat{\boldsymbol{\phi}}'_{mn,\pm}}{\partial x} = P_{mn}[M_{mn}\hat{\boldsymbol{\phi}}'_{mn,\pm} + \hat{\boldsymbol{g}}_{mn}(\boldsymbol{\phi}'_\pm)], \tag{2}$$

for $m = 0, \ldots, M$ and $n = -N, \ldots, N$. We note that $\boldsymbol{\phi}'_\pm$ must be real-valued, which yields the constraint $\hat{\phi}'_{mn,\pm} = \overline{\hat{\phi}'_{-mn,\pm}}$, so that we need only track $(M+1) \times (2N+1)$ Fourier modes. We can additionally introduce a spanwise symmetry condition, as described in Sleeman et al. (2025), which further reduces the number of modes to $(M+1) \times (N+1)$ [15]. Lin and Schmidt recently performed a study involing LES of K-type transition where they demonstrated that the flow stops being symmetric prior to the skin friction maximum [10]. With this in mind, we performed the NOWNS calculations for K- and H-type transition both with and without the symmetry condition and found that the calculation was not affected.

## 2 Results

Blowing/suction strips have often been invoked in numerical transition studies (e.g. [4, 13, 12]). NOWNS allows these strips to be included [15], whereas NPSE does not, although the effect of the strip can be modeled using Herbert's secondary stability theory to obtain an inlet boundary condition [5, 6, 1, 3, 2]. Here we use this approach

to study K-type (fundamental) and H-type (subharmonic) transition, with the goal of reproducing the DNS results of Sayadi et al. (2013) [14].

To approach the incompressible limit, we choose $\mathrm{Ma}_\infty = 0.1$, while we use the dimensionless quantities $\mathrm{Re}_x = \frac{\rho^*_\infty U^*_\infty x^*}{\mu^*_\infty}$, $y = \frac{y^*}{\delta^*_0}$, $F = \frac{\omega^* \mu^*_\infty}{\rho^*_\infty U^{*2}_\infty}$, and $b = \frac{\beta^* \mu^*_\infty}{\rho^*_\infty U^*_\infty}$, as well as the $u$-velocity amplitudes defined in Sleeman et al. (2025) [15]. Here the superscript $*$ denotes a dimensional quantity and the subscript $\infty$ denotes the free-stream value, while $\rho$ is the density, $U$ is the streamwise velocity of the baseflow, $\mu$ is the dynamic viscosity, $\omega$ is the temporal frequency, and $\beta$ is the spanwise wave number.

### 2.1 K-type transition

For K-type transition, we use the blowing/suction function specified in Rigas et al. (2021) [12], which matches that used by Rist and Fasel (1995) [13]. We use

$$f(x,z,t) = 5 \times 10^{-3} \sin(\omega t) v_a(x) + 1.3 \times 10^{-4} \cos(\beta z) v_s(x), \tag{3}$$

where

$$v_a(x) = \begin{cases} 0, & \mathrm{Re}_x \le \mathrm{Re}_x(x_1) \\ 15.1875\xi^5 - 35.4375\xi^4 + 20.25\xi^3, & \mathrm{Re}_x(x_1) < \mathrm{Re}_x \le \mathrm{Re}_x(x_m) \\ -v_a\big(2\mathrm{Re}_x(x_m) - \mathrm{Re}_x\big), & \mathrm{Re}_x(x_m) < \mathrm{Re}_x \le \mathrm{Re}_x(x_2) \\ 0, & \mathrm{Re}_x(x_2) < \mathrm{Re}_x \end{cases} \tag{4a}$$

$$v_s(x) = \begin{cases} 0, & R \le \mathrm{Re}_x(x_1) \\ -3\xi^4 + 4\xi^3, & \mathrm{Re}_x(x_1) < \mathrm{Re}_x \le \mathrm{Re}_x(x_m) \\ v_s\big(2\mathrm{Re}_x(x_m) - \mathrm{Re}_x\big), & \mathrm{Re}_x(x_m) < \mathrm{Re}_x \le \mathrm{Re}_x(x_2) \\ 0, & \mathrm{Re}_x(x_2) < \mathrm{Re}_x \end{cases} \tag{4b}$$

where $x_m = (x_1 + x_2)/2$, and $\xi = (\mathrm{Re}_x - \mathrm{Re}_x(x_1))/(\mathrm{Re}_x(x_m) - \mathrm{Re}_x(x_1))$. We choose the parameters $\mathrm{Re}_x(x_1) = 1.36 \times 10^5$, $\mathrm{Re}_x(x_2) = 1.56 \times 10^5$, $F = 110 \times 10^{-6}$ and $b = 0.419 \times 10^{-3}$ to match Sayadi et al. (2013) [14]. We further choose $M = 4$ temporal modes and $N = 8$ spanwise modes, with 1300 stations over the streamwise domain $\mathrm{Re}_x \in [1.36{\times}10^5, 2.73{\times}10^5]$, and 100 grid points in the wall-normal direction for $y \in [0, 60]$.

Figure 1a shows excellent agreement between the $u'$ amplitudes of NOWNS and the DNS of Sayadi et al. (2013) [14]. We note that in the early stages of the march there is disagreement between the DNS and NOWNS calculations because the blowing/suction strip causes upstream effects that NOWNS neglects by construction. However, these disturbances are convective in nature, and the amplitudes predicted by NOWNS rapidly converge to those predicted by DNS as the march progresses downstream. Figure 2 shows that NOWNS correctly predicts the initial rise in the skin friction coefficient, but following the initial rise, the NOWNS predicts a much more rapid growth of the skin friction than DNS, before eventually failing to converge. Figure 3a shows the $u$-velocity contours at $y/\delta_{\mathrm{inlet}} = 0.6$, as in Sayadi et al. (2013). We observe the aligned $\Lambda$-vortex structure that is characteristic of K-type transition, and good qualitative agreement with Sayadi et al. (2013) [14].

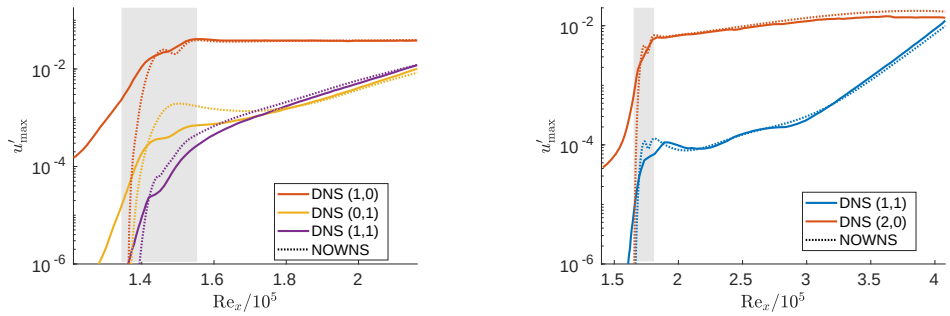


(a) Amplitudes for K-type transition

(b) Amplitudes for H-type transition

Fig. 1: Amplitudes for K- and H-type transition, compared to the DNS of Sayadi et al. (2013) [14].

### 2.2 H-type transition

For H-type transition we use the blowing/suction strip function

$$f(x,z,t) = 1.5\times10^{-3}\sin(2\omega t)v_a(x) + 1.5\times10^{-5}\sin(\omega t)\cos(\beta z)v_a(x), \qquad (5)$$

where for $v_a(x)$ defined in (4a). We choose $\mathrm{Re}_x(x_1) = 1.65\times10^5$ and $\mathrm{Re}_x(x_2) = 1.81\times10^5$, with $2F = 124\times10^{-6}$ and $b = 0.419\times10^{-3}$. We choose $M = 8$ temporal modes and $N = 14$ spanwise modes, with 2370 stations over the streamwise domain $\mathrm{Re}_x \in [1.65\times10^5, 5.16\times10^5]$, and 100 grid points in the wall-normal direction for $y \in [0, 60]$. Figure 1b plots the $u$-velocity amplitudes, while figure 2 plots the skin friction coefficient. We additionally plot the $u$-velocity contours in figure 3b, where we observe the staggered $\Lambda$-vortex structure characteristic of H-type transition.

## 3 Conclusions

We have demonstrated that NOWNS accurately simulates the early stages of transition by matching the $u$-velocity amplitudes predicted by DNS, while correctly predicting the initial rise in the skin friction coefficient, showing that NOWNS can be used to predict transition onset analytically. Doubling the resolution in $M$ and $N$ does not appreciably change the results, nor does it allow NOWNS to march farther downstream. Future work will investigate how the routine can be modified to better agree with DNS in the later stages of transition. In addition, we will apply NOWNS to high-speed boundary-layer flows.

**Acknowledgements** This work has been supported by The Boeing Company through the Strategic Research and Development Relationship Agreement CT-BA-GTA-1.

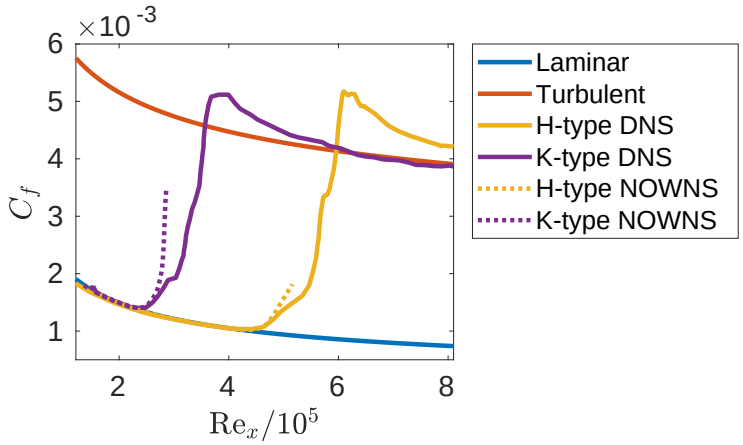


Fig. 2: Skin friction coefficient for K- and H-type transition, compared to the DNS of Sayadi et al. (2013) [14].

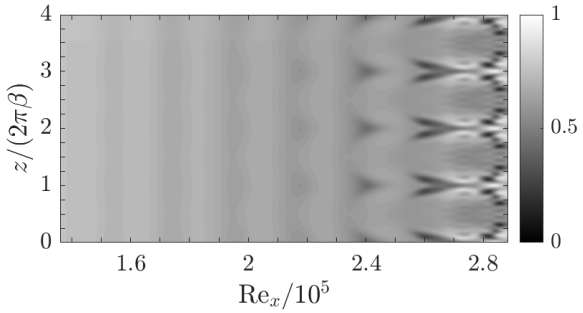


(a) K-type

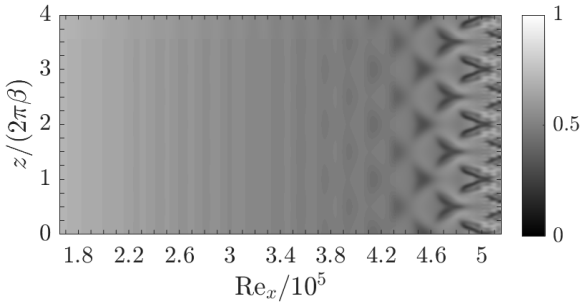


(b) H-type

Fig. 3: $u$-velocity contours at $y/\delta_{\text{inlet}} = 0.6$ for K- and H-type transition.

## References


1. Bertolotti, F.P.: Linear and nonlinear stability of boundary layers with streamwise varying properties. Ph.D. thesis, The Ohio State University (Jan 1991)
2. Chang, C.L., Malik, M.R.: Oblique-mode breakdown and secondary instability in supersonic boundary layers. J. of Fluid Mech. **273**, 323–360 (1994). https://doi.org/10.1017/S0022112094001965
3. Chang, C.L., Malik, M.R., Erlebacher, G., Hussaini, M.Y.: Linear and nonlinear PSE for compressible boundary layers. NASA Contractor Report 191537. Institute for Computer Applications in Science and Engineering (ICASE) (September 1993)
4. Fasel, H.F., Rist, U., Konzelmann, U.: Numerical investigation of the three-dimensional development in boundary-layer transition. AIAA J. **28**(1), 29–37 (1990). https://doi.org/10.2514/3.10349
5. Herbert, T.: Secondary instability of boundary layers. Ann. Rev. of Fluid Mech. **20**(1), 487–526 (1988). https://doi.org/10.1146/annurev.fl.20.010188.002415
6. Herbert, T.: Parabolized stability equations. Ann. Rev. of Fluid Mech. **29**(1), 245–283 (1997). https://doi.org/10.1146/annurev.fluid.29.1.245
7. Kamal, O., Rigas, G., Lakebrink, M., Colonius, T.: Input/output analysis of hypersonic boundary layers using the One-Way Navier-Stokes (OWNS) equations. In: AIAA AVIATION (June 2021). https://doi.org/10.2514/6.2021-2827
8. Kamal, O., Rigas, G., Lakebrink, M.T., Colonius, T.: Application of the One-Way Navier-Stokes (OWNS) equations to hypersonic boundary layers. In: AIAA AVIATION 2020 FORUM (June 2020). https://doi.org/10.2514/6.2020-2986
9. Kamal, O., Rigas, G., Lakebrink, M.T., Colonius, T.: Input/output analysis of a Mach-6 cooled-wall hypersonic boundary layer using the One-Way Navier-Stokes (OWNS) equations. In: AIAA AVIATION (June 2022). https://doi.org/10.2514/6.2022-3556
10. Lin, C., Schmidt, O.: Modal decomposition of K-type boundary layer transition. In: AIAA SCITECH (January 2024). https://doi.org/10.2514/6.2020-2986
11. Rigas, G., Colonius, T., Beyar, M.: Stability of wall-bounded fows using one-way spatial integration of Navier-Stokes equations. In: 55th AIAA Aero. Sci. Meet. (January 2017). https://doi.org/10.2514/6.2017-1881
12. Rigas, G., Sipp, D., Colonius, T.: Nonlinear input/output analysis: application to boundary layer transition. J. of Fluid Mech. **911**, A15 (2021). https://doi.org/10.1017/jfm.2020.982
13. Rist, U., Fasel, H.: Direct numerical simulation of controlled transition in a flat-plate boundary layer. J. of Fluid Mech. **298**, 211–248 (1995). https://doi.org/10.1017/S0022112095003284
14. Sayadi, T., Hamman, C.W., Moin, P.: Direct numerical simulation of complete H-type and K-type transitions with implications for the dynamics of turbulent boundary layers. J. of Fluid Mech. **724**, 480–509 (2013). https://doi.org/10.1017/jfm.2013.142
15. Sleeman, M.K., Colonius, T., Lakebrink, M.T.: Boundary-layer stability analysis using the Nonlinear One-Way Navier–Stokes Approach. AIAA J. **0**(0), 1–15 (2025). https://doi.org/10.2514/1.J064909
16. Towne, A., Colonius, T.: One-way spatial integration of hyperbolic equations. J. of Comp. Phys. **300**, 844–861 (2015). https://doi.org/10.1016/j.jcp.2015.08.015
17. Towne, A., Rigas, G., Kamal, O., Pickering, E., Colonius, T.: Efficient global resolvent analysis via the One-Way Navier–Stokes equations. J. of Fluid Mech. **948**, A9 (2022). https://doi.org/10.1017/jfm.2022.647